

BIOPHOTONICS

https://doi.org/10.1070/QEL16204

Monte Carlo simulation of a biological object with optical coherent tomography structural images using a voxel-based geometry of a medium

S.V. Frolov, A.Yu. Potlov, D.A. Petrov, S.G. Proskurin

Abstract. **We describe a Monte Carlo algorithm for simulating an interference signal and constructing a structural image of a biological object using optical coherent tomography (OCT). The algorithm is specific in that the object geometry is described by using a three-dimensional array of voxels combined into parallelograms, and the border cross checking is carried out by using an improved Smith algorithm. The geometry of the simulated object is reconstructed based on the structure of real biological tissues obtained by OCT. The algorithm efficiency is estimated by comparing experimental and corresponding simulated images of a subcutaneous blood vessel and upper layer of human skin *in vivo*.**

Keywords: *optical coherent tomography, coherent probing depth, blood vessels, Monte Carlo modelling, voxel-based model.*

1. Introduction

To date, optical coherent tomography (OCT) is a most promising and rapidly developing method for determining the internal structure of biological objects. The employment of OCT for medical and biological investigations was demonstrated in 1991 [1] and since that time, OCT has been widely used both in scientific-research purposes and in clinical biomedical diagnosis [2].

OCT permits obtaining high spatial resolution (3–20 μm) images of the internal structure of a medium; however, the coherent probing depth (CPD) is in this case limited by several millimetres. A particular CPD value varies depending on the employed scanning method and object under investigation; the maximal CPD is reached in studying eye retina [3]. In dermatologic studies, the CPD is only 1–2 mm, which is related to a high scattering coefficient of biological tissues [4–7]. Since one of the main factors limiting a greater CPD is the scattering of light (due to its influence on the formation of a detectable interference signal), it is necessary to obtain a comprehensive idea of the properties underlying the CPD. The corresponding computer simulation can solve this problem.

The most accurate description of light propagation in biological tissues is based on the method of multiple realisations of stochastic processes. The MCML package, which realises this approach, has been the public domain software since the middle 1990s [8]. In MCML, the free distance s covered by a photon package between the points of interaction with a medium is determined by the scattering (μ_s) and absorption (μ_a) coefficients:

$$s = \frac{-\ln \xi}{\mu_a + \mu_s}, \tag{1}$$

where ξ is a random number uniformly distributed between 0 and 1, which corresponds to the discrete character of energy absorption when the statistical weight of the photon package W at each of these points reduces by the value ΔW:

$$\Delta W = W \frac{\mu_a}{\mu_a + \mu_s}. \tag{2}$$

The scattering of light is described by using the Henyey–Greenstein phase function:

$$p(\cos\theta) = \frac{1 - g^2}{2(1 + g^2 - 2g\cos\theta)^{3/2}}, \tag{3}$$

where θ is the angle of scattering; g is the anisotropy factor for a medium.

The main drawback of MCML is that the simulation is only possible in a multilayer medium with plane boundaries, which allows one to describe real biological objects only in an approximate form. The MCML-based algorithm is continuously improved to increase the rate of simulation and correspondence to real biological systems.

Modern methods for describing a spatial object structure used for simulating photon migration are divided into several basic types. The first type implies the internal object structure presented in an analytical form including simplest geometrical figures [9, 10]. The second type considers an object as a set of three-dimensional segments, each of them being characterised by the corresponding optical properties [11–15]. The third type is based on presenting a medium as a polygonal mesh similarly to computer graphics [16–19].

The simulation algorithm of photon migration (after the corresponding improvement) can be used as a basis for OCT modelling. In 1999, a simplest algorithm of OCT modelling was presented. It was based on MCML in a homogeneous medium with employment of the essential sample method, which substantially increased the calculation rate [20]. Modelling of more complicated media implies either voxelisation (dividing an object to a great number of segments of known geometry) or the employment of a polygonal mesh. In the case of voxelisation, a detailed description of the medium requires a great number of voxels,

S.V. Frolov, A.Yu. Potlov, D.A. Petrov, S.G. Proskurin Tambov State Technical University, ul. Sovetskaya 106, 392000 Tambov, Russia; e-mail: zerner@yandex.ru

Received 11 September 2016; revision received 21 March 2017
Kvantovaya Elektronika **47** (4) 347–354 (2017)
Translated by N.A. Raspopov

which means a multitude of border cross checking procedures for photons with the voxel's faces. However, voxelisation provides the fast transfer from a structure image (obtained, for example, via the magneto-resonance or computer tomography) to the geometry of a medium for simulation [12, 13, 15].

The employment of a polygonal mesh for forming a medium structure allows one to specify orientation of object faces more exactly than in the case of voxelisation, because the planes forming the boundaries may have various angles with respect to each other. Nevertheless, in some cases this approach implies a great number of border cross checking procedures, because the number of polygons forming the boundary may be rather great [16, 17]. However, the border cross checking procedure is simpler when the object is divided to tetrahedrons [19]. This approach is known from [21], where several thousand tetrahedrons have been used for forming the geometry of a biological object in question.

For modelling structural images in the frequency domain there exists an approach based on obtaining the wavelength-dependent boundary signals, to which a Fourier transform is applied for obtaining A-scans of the structure image [22]. In this case, the signal of the object interferometer arm is

$$S(k) = \sqrt{G(k)} \sum_{n=1}^{N} \sqrt{R_n} \exp(\mathrm{i}2kl_n), \quad (4)$$

where R_n is the statistical weight of the nth photon package; l_n is the distance covered by the nth photon; k is the wave-number; and $G(k)$ is the Gaussian spectrum of the light source. The boundary signal is obtained from the formula

$$I_D(k) = |S(k) + R(k)|^2 - |S(k) - R(k)|^2, \quad (5)$$

where $R(k)$ is the signal of the reference interferometer arm. The principal difference between the time-domain and spectrum-domain simulation lies in the process of forming the structural image. In this case, the behaviour of optical radiation propagation is similar in both cases.

There are algorithms [23, 24], capable of sufficiently exactly describing the time-domain process of interference signal detection. In simulation, the light intensity $I(z)$ detected by a sensor is described by the formula:

$$I(z) = I_0 \sum_{i=1}^{N} \sqrt{W} \exp\left[-\left(\frac{2z - L_i}{l_{coh}}\right)^2\right] \cos\left[\frac{2\pi}{\lambda}(2z - L_i)\right], \quad (6)$$

where I_0 is a constant determined by the OCT system; W is the statistical weight of the photon package outgoing from tissue inside the domain of the sensor placement; L_i is the optical path covered by the photon package; λ is the source wavelength; z is the optical path in the reference interferometer arm;

$$l_{coh} = \frac{2\ln 2}{\pi} \frac{\lambda^2}{\Delta\lambda} \quad (7)$$

is the coherence length; and $\Delta\lambda$ is the FWHM spectral width.

The present work is aimed at developing the simulation algorithm for the time-domain interference signal by the Monte Carlo method of statistical tests, which might reveal and study specific features of the formation of structural images for strongly scattering media with a complicated spatial structure.

2. Simulation of the geometry and optical properties of an investigated biological object

As a rule, biological objects have a sophisticated spatial structure, which may not always be described analytically. In modelling structural OCT images, this fact is especially important because the boundaries of medium inhomogeneities conventionally have a complicated geometry, especially at a high spatial resolution. Hence, for enhancing the adequacy of simulation results it is reasonable to use the approach capable of describing the internal structure of a biological object most exactly. We suggest the employment of a voxel-based model for forming the model medium and the corresponding approach for describing photon propagation in this medium.

The internal structure of the biological object in question we will present as a set of 3D elements (voxels), each of them having specific optical characteristics (the scattering coefficient μ_s, absorption coefficient μ_a, index of anisotropy, and refractive index n). The total number of voxels in a certain direction N is determined issuing from the size of the sample under study, l, in this direction:

$$N = l/d, \quad (8)$$

where d is the size of a voxel edge. In a general case, the number and length of voxel edges in the x and y axes may differ from the corresponding value in the z axis.

In the basic variant, the internal structure of the object is constructed by using OCT images obtained previously (Fig. 1a). However, the images may be obtained by other methods of medical visualisation and even by simplified schemes of biological object geometry (analytically or manually formed images). In both the cases, voxels of the modelled medium are formed on the basis of pixels of the structural image. Some structures of the investigated object, that is, types of biological tissues such as blood, epidermis, derma, and so on, can be separated by using various algorithms. For example, one can employ the authors' algorithm [25] based on isohel (posterisation) of a structural image with the following coding of separated structures. A reduction of the quantisation levels for the initial image reduces the number of half-tones to a required level (as a rule, several dozen). This, on the one hand, allows one to describe optical and geometrical characteristics of the object under study with ~90% confidence, and, on the other hand, quickly identify tissues (to put them into correspondence with certain optical characteristics) even in the manual regime. In most cases, such an approach gives a chance to allocate only one memory byte per voxel for storing the tissue identifier (Fig. 1b) and address the optical characteristics through a separate array. If the simulation is based on a single B-scan, then the distribution of optical characteristics over all cross sections in the y axis is either assumed in a simplified form, similar to that of the initial structural image (for example, for the refractive index $n_{x,y,z} = n_{x,y+1,z} = \ldots = n_{x,N_y,z}$, where x, y, z are the coordinates of voxels, N_y is the total number of voxels along the y axis) (Fig. 1e), or corrected according to the assumed structure of the biological object. The approach suggested allows one to use an arbitrary graphical image as a basis for forming the object structure in simulation, which gives a chance to describe an arbitrarily complicated medium.

The main drawback of the classical voxel approach is the necessity of specifying a great number of voxels for a suf-

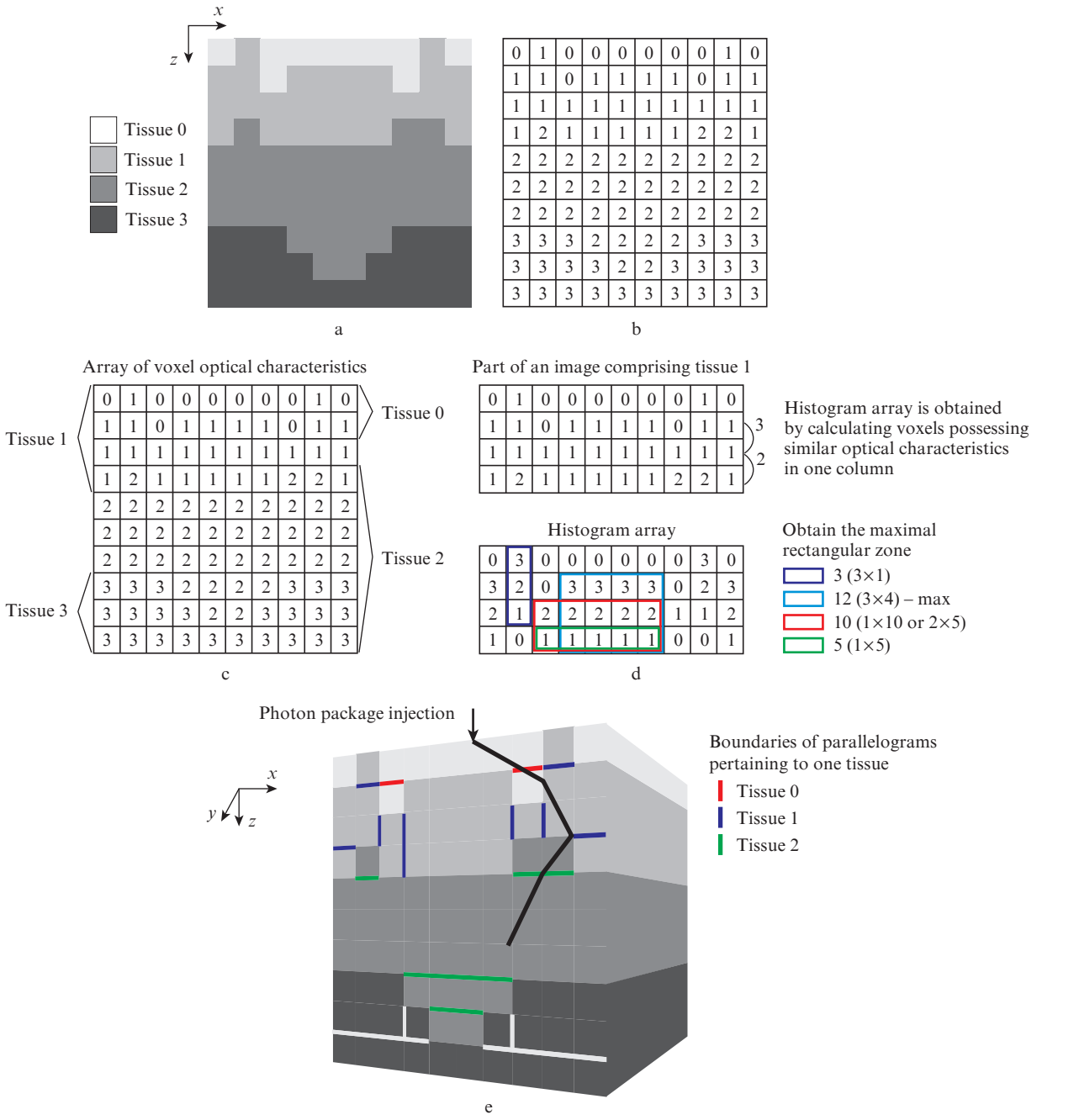

Figure 1. Scheme of constructing the internal structure of an investigated biological object for modelling. A tomogram of an investigated biological object (a) is a basis for the main cartogram (b), in which structures of the biological object are coded taking into account their geometrical position and optical characteristics. For obtaining a 3D geometrical model, the maximal rectangular zone is searched for the voxels possessing similar optical characteristics, which are then combined. Results of the localisation of tissue boundaries (c) and obtained histogram arrays (d) used for searching for the maximal rectangular zone are shown. The formed 3D geometrical model of a biological tissue (e) is presented as the medium comprised of sets of parallelograms. Boundaries of the parallelograms with similar optical characteristics (e) are shown in grey scale.

ficiently exact description of the medium with complicated geometry of boundaries. In this case, the number of necessary voxel border cross checking procedures increases. Such procedures are needed even in the case where photon passes into a voxel possessing the same optical characteristics or if at least one of neighbouring voxels has distinct characteristics. To simplify calculations, we suggest using the technique of joining neighbouring voxels with similar optical characteristics into one massive parallelepiped. In this way, the problem of reducing the number of needed border cross checking procedures reduces to dividing the medium into an optimal number of segments, which we assume to form by finding the largest rectangular zones possessing similar optical characteristics.

At a first stage, tissue boundaries are localised, that is, the first and last voxels are searched for in the vertical and horizontal directions with the index of this tissue. It is needed for minimising the spatial search for the greatest zone (Fig. 1c). Then, the histogram array is formed for each column by calculating the number of neighbouring voxels possessing similar optical characteristics in one column (Fig. 1d). From the histograms obtained, the maximal rectangular zone is determined. Then indices of the voxels inside this zone are zeroed

in order to exclude them from the calculation of the next maximal rectangular zone. The process is repeated until the zone comprising a single voxel remains. Then, the search for other tissue type is performed. As a result result, the modelled medium will be presented by a set of parallelepipeds (Fig. 1e) so that the number of needed border cross checking procedures will sufficiently reduce, which, in turn, will substantially increase the rate of simulation as compared to the classical voxelisation, when the medium is divided into a great number of voxels [11–15]. In what follows, under voxels we assume the parallelograms obtained due to joining.

3. Simulation of propagation of light in a medium with voxel geometry

The process of photon propagation inside an investigated object comprises the following specific features: photon input, determining the free path, condition for fulfilment of border cross checking, scattering and absorption (Fig. 2).

When a photon starts up, its initial position and direction of motion should be determined (issuing from the type of the employed radiation source). In the case of the most simple simulation, a point source is used, and the initial position of the photon is determined by the number A_i of a current A-scan and by distance d between neighbouring A-scans:

$$x_i = x_0 + A_i d, \quad y_i = y_0, \quad z_i = 0, \tag{9}$$

where x_0 and y_0 are the coordinates of the source initial position (the point, from which the sample scanning starts).

The radiation source used in OCT can be approximately presented as a Gaussian beam, for which the probability density for the photon package to fit a certain radial position is determined [26] as

$$p(r) = \frac{4r}{w_0^2} \exp\left(\frac{-2r^2}{w_0^2}\right), \tag{10}$$

where w_0 is the beam radius. By adapting (10) to the Monte Carlo method, one obtains

$$r = \frac{w_0}{\sqrt{2}} \sqrt{-\ln \xi}, \tag{11}$$

where ξ is a random number uniformly distributed between 0 and 1. Then, the initial position of the photon package in modelling is

$$\begin{aligned} x_i &= \frac{w_0}{\sqrt{2}} \sqrt{-\ln \xi} \cos \varphi_{\text{az}} + A_i d, \\ y_i &= \frac{w_0}{\sqrt{2}} \sqrt{-\ln \xi} \sin \varphi_{\text{az}}, \\ z &= 0, \end{aligned} \tag{12}$$

where φ_{az} is the azimuth angle, which is calculated by using the random number ξ as well:

$$\varphi_{\text{az}} = 2\pi\xi. \tag{13}$$

In OCT simulation, it may be interesting to use a collimated Gaussian beam focused to a certain depth z_{f} inside the sample in question. In this case, the initial values of the direction cosines u_x, u_y, u_z [27] are as follows:

$$u_x = \frac{-x}{\sqrt{r^2 + z_{\text{f}}^2}}, \quad u_y = \frac{-y}{\sqrt{r^2 + z_{\text{f}}^2}}, \quad u_z = \frac{z_{\text{f}}}{\sqrt{r^2 + z_{\text{f}}^2}}. \tag{14}$$

For calculating the free path s between the points corresponding to the acts of interaction with a medium, we suggest using only the scattering coefficient,

$$s = \frac{-\ln \xi}{\mu_{\text{s}}}, \tag{15}$$

and calculate the energy absorption by the Bouguer–Lambert–Beer law:

$$W_{i+1} = W_i \exp(-\mu_{\text{a}} s), \tag{16}$$

where W_i, W_{i+1} are the photon statistical weights prior to and after absorption, respectively. This representation corresponds to the instantaneous absorption of the beam energy [in contrast to the discrete absorption, see (2)], which occurs after the photon makes a step by certain length s.

Scattering characterises the change in the photon motion direction and is calculated through the angle of scattering, determined by using the phase function (3) and the polar angle $\varphi = 2\pi\xi$, which is uniformly distributed from 0 to 1. The new values for the direction cosines are

$$\begin{aligned} u_x' &= \frac{\sin\theta(u_x u_z \cos\varphi - u_y \sin\varphi)}{\sqrt{1 - u_z^2}} + u_x \cos\theta, \\ u_y' &= \frac{\sin\theta(u_y u_z \cos\varphi - u_x \sin\varphi)}{\sqrt{1 - u_z^2}} + u_y \cos\theta, \\ u_z' &= -\sqrt{1 - u_z^2} \sin\theta \cos\varphi + u_z \cos\theta. \end{aligned} \tag{17}$$

In the voxel-based approach, a photon package starts to move in a certain segment of the medium array. After each determination of the photon free path between the interaction points, the border cross checking for the current voxel is performed by using the improved Smith algorithm:

$$\begin{aligned} b_x &= \begin{cases} \dfrac{x + d_x - x_{\text{c}}}{u_y} & \text{for } x_y > 0, \\ \dfrac{x - x_{\text{c}}}{x_y} & \text{for } x_y < 0, \end{cases} \\ b_y &= \begin{cases} \dfrac{y + d_y - y_{\text{c}}}{u_y} & \text{for } u_y > 0, \\ \dfrac{y - y_{\text{c}}}{u_y} & \text{for } u_y < 0, \end{cases} \\ b_z &= \begin{cases} \dfrac{z + d_z - z_{\text{c}}}{u_z} & \text{for } u_z > 0, \\ \dfrac{z - z_{\text{c}}}{u_z} & \text{for } u_z < 0. \end{cases} \end{aligned} \tag{18}$$

where b_x, b_y, and b_z are the distances to the planes comprising voxel edges; x_{c}, y_{c}, and z_{c} are the coordinates of the photon current position; d_x, d_y, and d_z are the edge lengths of the voxel; and x, y, z are the coordinates of the planes, in which the corresponding lower edges of the voxel comprising the photon lie:

$$z = c_z d_z, \quad y = c_y d_y, \quad x = c_x d_x \tag{19}$$

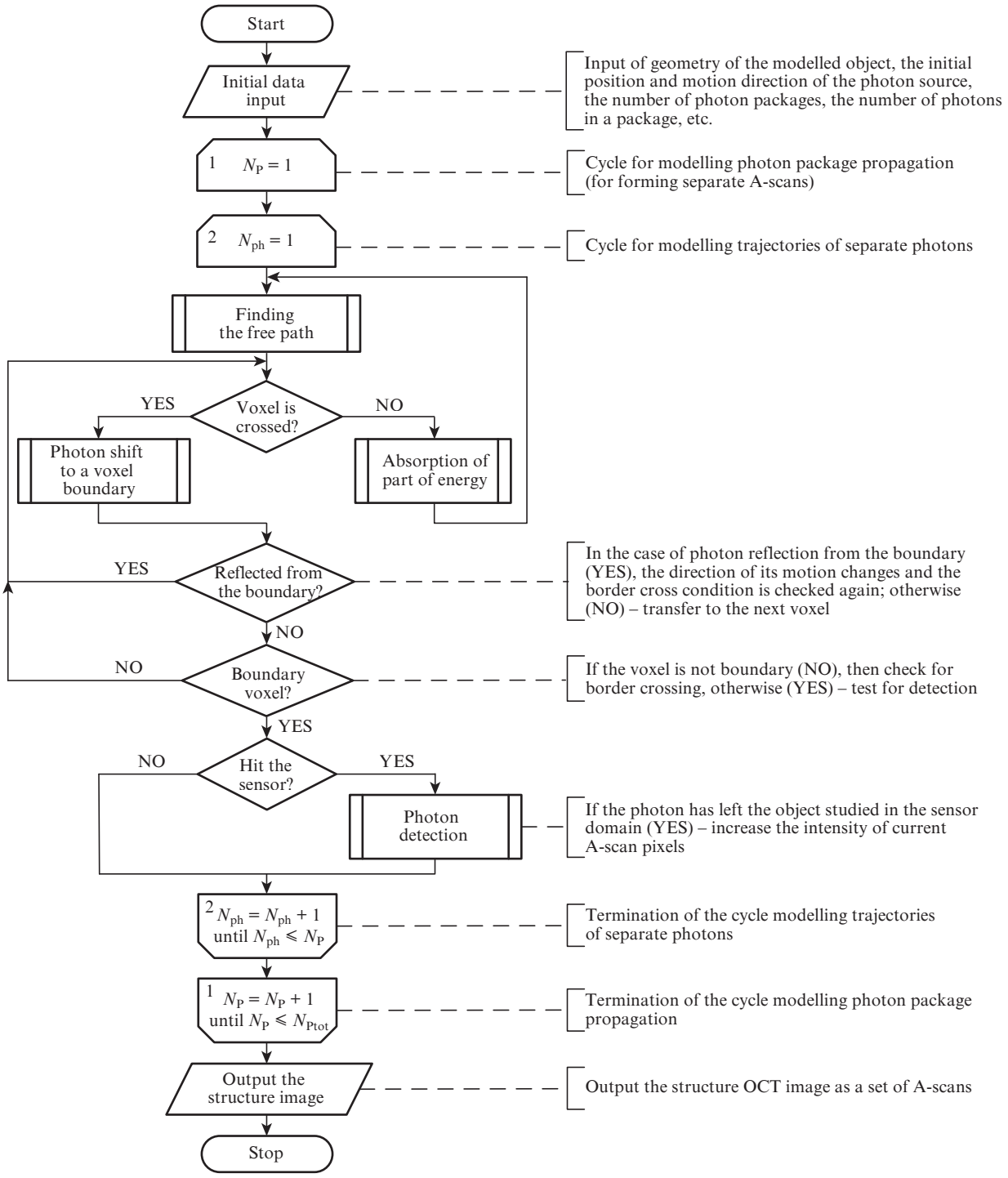

Figure 2. Main stages of the simulation algorithm for light propagation in a biological object. The radiation source and sensor alternately move along a medium boundary. Scanning is performed by introducing and detecting photons reflected from various optical irregularities.

(c_x, c_y, and c_z are the indices of the current voxel in the medium array). A distance to the edge, crossed by the photon is determined by comparing b_x, b_y, and b_z; then, the lowest value is compared to the free path. If the distance to the edge in the motion direction is less than this value, then the photon shifts to the voxel edge. If the refractive indices of the current voxel and the voxel into which the photon package passes differ, then the probability of border crossing is determined by the Fresnel formulae:

$$R = \frac{1}{2}\left(\frac{\sin^2(\alpha_{in} - \alpha_{ref})}{\sin^2(\alpha_{in} + \alpha_{ref})} + \frac{\tan^2(\alpha_{in} - \alpha_{ref})}{\tan^2(\alpha_{in} + \alpha_{ref})}\right), \quad (20)$$

where α_{in} is the angle of incidence; and α_{ref} is the angle of refraction. Then the value of R is compared to the random value $\xi \in [0,1)$; if $\xi > R$, then the photon passes to a next segment, and if $\xi \leqslant R$, then the photon reflects from the boundary. In the case where the photon passes into a paral-

lelogram possessing the same optical properties, the procedure is repeated for the new boundaries only. The photon moves again to an intersected boundary or moves along the rest distance and then a new free path length is calculated.

Note that the probe beam starts motion not inside a biological tissue, but outside it and crosses an air layer of a certain thickness. In the MCML algorithm, the variant where the absorption and scattering coefficients of the medium are zero is considered separately, because in the calculation of a free path the exclusive situation occurs, namely, division by zero. In the case of the voxel-based geometry of the medium, the number of necessary checking procedures substantially increases, which may reduce the rate of modelling. Hence, it is more convenient to take the scattering coefficient in air close to zero $\mu_s < 10^{-12}$ rather than zero. In using the Bouguer–Lambert–Beer law, the absorption coefficient may be zero; correspondingly, the optical characteristics for air, used in the simulation, are as follows: $\mu_s \leqslant 10^{-12}$ cm^{-1}, $\mu_a = 0$, $n = 1$, $g = 1$.

When the photon beam leaves the investigated medium inside the domain of the sensor position with the radius d_D and numerical aperture θ, its statistical weight is added to the intensity of the set of pixels of the current A-scan according to (6):

$$I'_{i,j} = \begin{cases} \sqrt{W}\exp\left[-\left(\dfrac{2z - L_i}{l_{coh}}\right)^2\right]\cos\left[\dfrac{2\pi(2z - L_i)}{\lambda}\right] \\ \qquad \text{for } u_z > \theta,\ r < d,\ |2z - L_i| < l_{coh}, \\ 0, \quad \text{if otherwise,} \end{cases} \tag{21}$$

where j is the index of the A-scan pixel. Equation (21) is used in the case where the modelling takes into account a speckle-structure of the OCT signal. If it is not the case, then the multiplier $\cos[2\pi(2z - L_i)/\lambda]$ in (21) can be replaced with unity. The condition $|2z - L_i| < l_{coh}$ means that the photon energy may be neglected if the photon optical path differs from the optical path in the reference arm by a value less than the coherence length [20, 21].

4. Results and discussion

The algorithm suggested is realised in C# language. Its adequacy was verified in a series of tests by modelling structural OCT images of real biological objects (Figs 3a and 4a). The modelling was performed in the two variants: with the speckle-structure of the OCT signal taken into account or neglected. The number of photons per each A-scan is $N_P \approx 10^7$, which corresponds to $N_P = 3.33\times10^6$ per each calculation stream (one stream corresponds to one processor core; three of the four cores of an Intel Core i5-4670 central processor operating at a frequency of 3.4 GHz were used in the calculations). The number of A-scans was 180.

The geometry of the medium used in the calculations is shown in Fig. 3b. It approximately reproduces the structure of human skin upper layers (Fig. 3a). The coherence length l_{coh} is 14.4 μm, the source wavelength is $\lambda = 1298$ nm, which corresponds to the experimental model presented in previous works [28]. The optical characteristics of tissues were obtained by averaging the corresponding data from [29–31] and are given in Table 1. The simulation results are shown in Figs 3c and 3d.

Generally, we may note visual similarities of the structural images obtained with the voxel-based model and from experi-

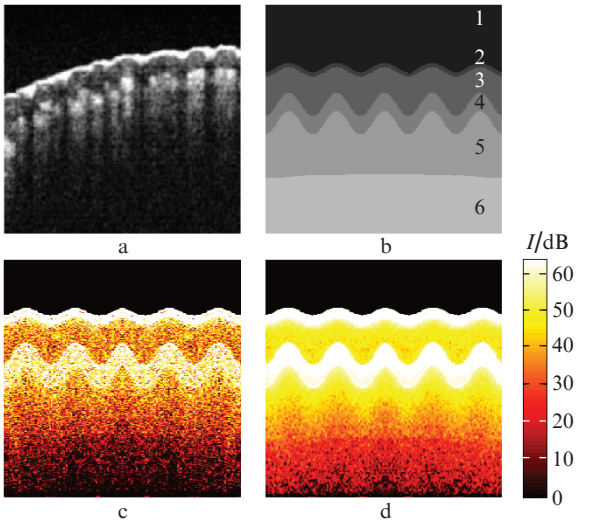

Figure 3. (a) Experimentally obtained [27] image of human skin upper layers *in vivo* and (b) the structure approximately corresponding to it formed for modelling. The result of modelling and the resulting structural OCT image for skin upper layers (see Table 1) with (c) neglected speckle-structure of the OCT signal and with (d) the speckle-structure taken into account. The image size is 2×2 mm.

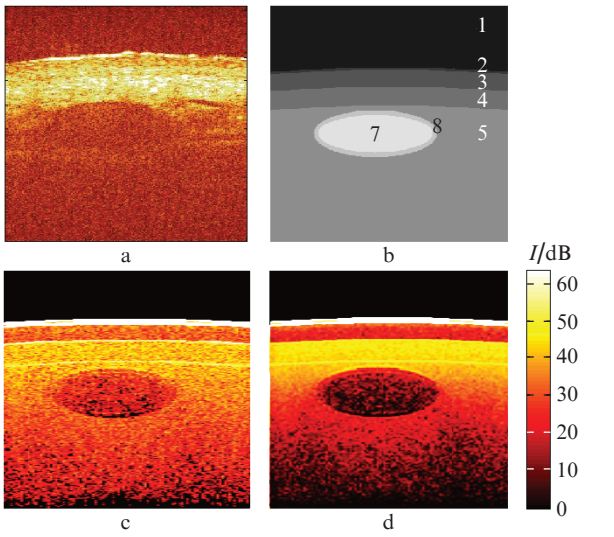

Figure 4. (a) Experimentally obtained image of human skin upper layers [7] with a blood vessel *in vivo* and (b) the structure approximately corresponding to it formed for modelling. The result of modelling the OCT image of the skin upper layers (see Table 1) with (c) neglected speckle-structure of the OCT signal and with (d) the speckle-structure taken into account. The image size is 2×2 mm.

Table 1. Optical characteristics of the upper layers of human skin.

Layer number	Medium	μ_s/cm^{-1}	μ_a/cm^{-1}	g	n
1	Air	0.0000001	0	1	1
2	Corneous layer	320	0.2	0.9	1.49
3	Top epidermis	63	0.3	0.93	1.37
4	Epidermis	120	0.6	0.87	1.38
5	Dermis	90	0.8	0.9	1.36
6	Germinative layer	110	1.1	0.9	1.35
7	Blood	650	2	0.995	1.37
8	Vascular wall	2.8	0.9	0.95	1.38

mental B-scans. Tissues possessing the lowest indices of anisotropy g and the highest scattering coefficients μ_s exhibit the highest image intensities. However, tissues with a high index of anisotropy, in which a comparatively small part of photons is reflected (scattered) backward, have relatively low intensity in the structural image. There is a specific feature of the images obtained by taking into account speckles, which is revealed as an increased granularity/noise of the image related to the interference of coherent optical light. The time needed for calculating one B-scan is ~253 min. A comparison of the structural images obtained in the approach of the present work and with models from [23, 24] confirms adequacy of the investigation results.

Especially interesting in biomedical investigations is visualisation of subcutaneous structures *in vivo*, such as saphenous blood vessels. Possible visualisation of such structures was demonstrated in previous works [7, 28]. Since blood has a high index of scattering, which is several times that of epidermis and dermis, the test for adequacy of the voxel-based OCT modelling is of particular interest in this case. In Fig. 4a one can see an experimental image of human skin upper layers with a saphenous blood vessel. A geometrical model of the medium is shown in Fig. 4b. The optical characteristics of the medium [29–31] are taken from Table 1. The simulation results are presented in Figs 4c and 4d. The radiation source parameters in simulation corresponded to those in the experiment: $\lambda = 1298$ nm, $\Delta\lambda = 52$ nm, which corresponds to $l_{coh} = 14.3$ μm; it is assumed that the collimated beam of photons has a Gaussian profile.

Results of simulation show that the images are mostly distinct in the contact points of two tissues possessing different refractive indices. This is related to the fact that in the voxel-based model, the reflection at the interface of two segments with different refractive indices is calculated relative to the normal oriented perpendicularly to the intersection plane; the set of normals determines the boundary between two tissues. In this case, the normal direction will coincide with that of the axis, which is perpendicular to the voxel edge intersected by the photon. When one prescribes the boundaries analytically, the reflection is calculated relative to the normal to the tangent plane at the point of beam incidence onto the surface prescribing the layer boundary.

The coefficient of correlation between the simulation results (Fig. 4c) and experimental image (Fig. 4a) is 0.66, which is related to peculiarities of prescribing the internal structure of the medium. A structure of the object for modelling shown in Fig. 5a was obtained directly from an experimental OCT image (Fig. 4a) by selecting the boundaries between various layers in the medium. Results of the simulation are shown in Figs 5b and 5c.

The coefficient of correlation between the experimental (Fig. 4a) and modelled (Fig. 5c) images is 0.85–0.95. The determination of the medium internal structure based on an experimentally obtained image allows one to obtain a substantially better similarity of the modelling results with experimental data.

The time needed for obtaining one image was about 270 min. In order to estimate the performance as compared to the classical voxel approach, the simulation was performed by employing a similar medium geometry by the algorithm from [12]. In the latter case, the time needed for obtaining one B-scan was 856 min.

5. Conclusions

An algorithm is presented for Monte Carlo simulation of a time-domain interference OCT signal with the employment of voxel-based geometry and the method of combining voxels for describing the internal structure of a biological object. The formation of the geometry of the object in question by using the images of the medium internal structure obtained with various methods of biomedical diagnostics was repeatedly implemented previously. However, in modelling structural OCT -images, experimental OCT images have not been used so far for direct formation of the medium structure and the following comparison of the results obtained to experimental data. Note that the algorithm suggested allows one to reach high adequacy of simulation results to physical experiments.

The employment of the method for combining voxels has increased the rate of modelling by several times as compared to the classical voxel-based approaches based on dividing a medium into numerous separate segments. The new approach is flexible and provides quick and simple transfer from the image possessing the geometry of the investigated biological object to the voxel-based model of the medium.

Despite the increased simulation rate, the current performance (270 min per B-scan) can be substantially improved, for example, by using parallel calculations. New investigations will be aimed at increasing the rate of simulation by modifying the suggested algorithm with the method of essential sampling.

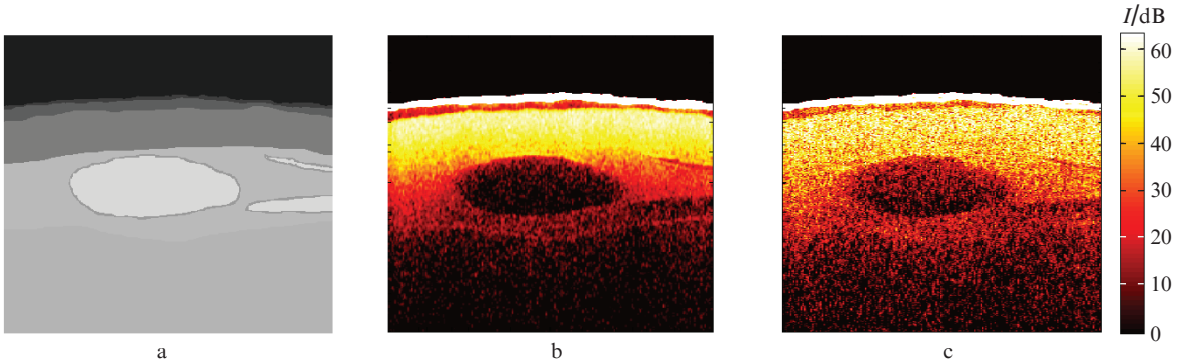

Figure 5. (a) Modelled medium structure obtained by transforming an experimental image and (b, c) the result of modelling the structural image of the subcutaneous blood vessel when the speckle-structure was (b) neglected or (c) taken into account.

Acknowledgements. The work was supported by the Russian Science Foundation (Project No. 16-15-10327).

References

1. Huang D. et al. *Science*, **254**, 1178 (1991).
2. Zysk A., Nguyen F., Oldenburg A., Marks D., Boppart S. *J. Biomed. Opt.*, **12** (5), 051403 (2007).
3. Fercher A.F., Drexler W., Hitzenberger C.K., Lasset T. *Rep. Prog. Phys.*, **66**, 239 (2003).
4. Tuchin V.V. *Tissue Optics: Light Scattering Methods and Instruments for Medical Diagnostics* (Bellingham: SPIE Press, 2007).
5. Zimnyakov D.A., Tuchin V.V. *Quantum Electron*., **32**, 849 (2002) [*Kvantovaya Elektron*., **32**, 849 (2002)].
6. Sattler E., Kastle R., Welzel J. *J. Biomed. Opt.*, **18** (6), 061224 (2013).
7. Proskurin S.G. *Quantum Electron*., **42**, 495 (2012) [*Kvantovaya Elektron*., **42**, 495 (2012)].
8. Wang L.H., Jacques S.L., Zheng L.Q. *Comput. Meth. Programs Biomed.*, **47** (2), 131 (1995).
9. Periyasamy V., Pramanik M. *J. Biomed. Opt.*, **19** (4), 045003 (2014).
10. Zhu C., Liu Q. *J. Biomed. Opt.*, **17** (1), 010501 (2012).
11. Fang Q.Q., Boas D.A. *Opt. Express*, **17** (22), 20178 (2009).
12. Kurihara K. et al. *Biomed. Opt. Express*, **3** (9), 2121 (2012).
13. Chuang C.C. et al. *Biomed. Eng. Online*, **11** (21) (2012).
14. Prefer T.J. et al. *J. Sel. Top. Quantum Electron.*, **2** (4), 934 (1996).
15. Boas D.A. et al. *Opt. Express*, **10** (3), 159 (2002).
16. Margallo-Balbas E., French P.J. *Opt. Express*, **15** (21), 14086 (2007).
17. Ren N.N. et al. *Opt. Express*, **18** (7), 6811 (2010).
18. Gorshkov A.V., Kirillin M.Yu. *J. Comput. Sci.*, **3** (6), 498 (2012).
19. Fang Q.Q. *Biomed. Opt. Express*, **1** (1), 165 (2010).
20. Yao G., Wang L.V. *Phys. Med. Biol.*, **44** (9), 2307 (1999).
21. Malektaji S., Lima T., Sherif S. *J. Biomed. Opt.*, **19** (4), 046001 (2014).
22. Hartinger A.E., Nam A.S., Chico-Calero I., Vakoc B.J. *Biomed. Opt. Express*, **5** (12), 4338 (2014).
23. Kirillin M., Meglinski I., Kuzmin V., Sergeeva E., Myllylä R. *Opt. Express*, **18** (21), 21714 (2010).
24. Kirillin M.Yu., Priezzhev A.V., Myllylä R. *Quantum Electron*., **38**, 570 (2008) [*Kvantovaya Elektron*., **38**, 570 (2008)].
25. Potlov A.Yu., Proskurin S.G., Frolov S.V. Svidetel'stvo o gosregistratsii programmy dlya EVM No. 20166113996 (Certificate of State Registration of Computer Software No. 20166113996) (12 April 2016).
26. Koprowski R., Wrobel Z. *Adv. Intelligent Soft Comput.*, **57**, 471 (2009).
27. Tycho A., Bjarklev A.O. *Ph.D. Thesis* (Denmark, 2002).
28. Proskurin S.G., Vang R.K. *Quantum Electron*., **34**, 1157 (2004) [*Kvantovaya Elektron*., **34**, 1157 (2004)].
29. Bashkatov A.N., Genina E.A., Kochubey V.I., Tuchin V.V. *J. Phys. D: Appl. Phys.*, **38** (15), 2543 (2005).
30. Salomatina E., Jiang B., Novak J., Yaloslavsky A.N. *J. Biomed. Opt.*, **11** (6), 064026 (2006).
31. Gemert M.J.C., Verdaasdonk R., et al. *Las. Surgery Med.*, **5**, 235 (1985).